Morphology and Physical Properties of Au-doped Zinc Oxide by Pulsed Laser Deposition

BY

Jelani Hernandez Hannah

B.A., Fisk University, 2011

THESIS

Submitted as partial fulfillment of the requirements

for the degree of Master of Science in Mechanical Engineering

in the Graduate College of the

University of Illinois at Chicago, 2014

Chicago, Illinois

Defense Committee:

Dr. Jeremiah T. Abiade, Chair and Advisor, Mechanical and Industrial Engineering

Dr. Carmen Lilley, Mechanical and Industrial Engineering

Dr. Amin Salehi-Khojin, Mechanical and Industrial Engineering

ACKNOWLEDGEMENTS

I would like to give my highest gratitude and appreciation to the Creator (God) for allowing me to reach this point in success. I would like to thank my parents Dr. Paul Hannah and Dr. Martha Hernandez for their continued support and encouragement through all my years of scholastic endeavors. I also want to give thanks to my advisor Dr. Jeremiah T. Abiade for his guidance and support for allowing me to pursue my research and scientific inquiries. Finally, I want give to thanks to my colleagues in the Laboratory for Oxide Research and Education (LORE) Riad Alzghier, Sin Pui-Fu, Chen Chen and Chenlin Zhao as well as my respected committee members Dr. Carmen Lilley and Dr. Amin Salehi-Khokin as well as Dr. Ke-Bin Low at the University of Illinois at Chicago Research Resource Center and all collaborators at the Materials Research Laboratory at University of Illinois at Urbana-Champaign.

CONTRIBUTION OF AUTHORS

Chapter 1 serves as introduction to theory and significance of this research, relating to industry and fundamental science. Chapter 2 is a literature review that places my thesis question in the context of the larger field and highlights the significance of my research question. Chapter 3 lists all experimental procedures with generated figures, tables and equations that played a large role in the writing of this thesis along with my research mentor and advisor, Dr. Jeremiah Abiade. Chapter 4 represents a series of my own unpublished experimental results directed at answering the question of physical properties of Au-doped zinc oxide thin films. I anticipate that this line of research will be continued in the laboratory after I leave and that this work will ultimately be published as part of a co-authored manuscript. Chapter 5 & Chapter 6 represents my synthesis of the research presented in this thesis and my overarching conclusions. The future directions of this field and this research question are discussed.

TABLE OF CONTENTS

CHAPTER **PAGE**

LIST OF TABLES

TABLE **PAGE**

LIST OF EQUATIONS

EQUATION **PAGE**

LIST OF FIGURES

FIGURE **PAGE**

LIST OF ABBREVIATIONS

LED	Light Emitting Diode
PLD	Pulsed Laser Deposition
XPS	X-Ray Photoelectron Spectroscopy
XRD	X-Ray Diffraction
PL	Photoluminescence
TEM	Transmission Electron Microscopy
ZnO	Zinc Oxide
V_o	Oxygen vacancy
Zn_i	Zinc interstitial
eV	Electron volt
nm	Nanometer
Au	Gold
K	Kelvin
UV	Ultraviolet

SUMMARY

In the effort to realize the potential for reliable p type ZnO with group 1B dopants using Au as active acceptor impurity; the morphology and change in physical properties of thin films grown on c-plane sapphire substrate by pulsed laser deposition was investigated. Deposited Au-doped ZnO thin films resulted in formation of heterogeneous Au-ZnO crystal structure with high hexagonal c-axis orientation to c-plane sapphire substrate. Theoretical suggestions of Au_{zn} cationic defects in ZnO were confirmed by formation of Au-O bonds and absence of intermetallic AuZn bonds using XPS. Complementary structural characterization by x-ray diffraction demonstrated the presence of Au (111) and crystalline ZnO (002) peaks with absence of intermetallic AuZn phase. Au was realized to be soluble in ZnO with formation of multiphase film by high atomic interdiffusion exceeding the solute solubility limit. Primary PL results suggest deep and shallow defect level as indicated by shifts broad and narrow energy band transitions present in both 300 K and 80 K peaks, suggesting migration and dominant Au impurity defect levels in ZnO band gap.

Chapter 1: Introduction

In the expanding information and technology age, global use of semiconductor devices provide unwavering optimism for the forthcoming new generation of electronic devices. Silicon has revolutionized electronic devices over the past 60 years. However, silicon has limited optoelectronic properties due to its indirect band gap. Use of direct band gap materials is the next step for enhanced device efficiency and processing in light emitting diode (LED) and lighting applications. Particularly II-VI semiconductors are attractive due to their green, blue and UV light emission and high thermal tolerance. Among the semiconductors, zinc oxide is a highly attractive with its large exciton binding energy of 60 meV at room temperature which makes ZnO attractive LED device. In addition to robust optoelectronic properties, ZnO has been investigated for years for applications in biomedical, spintronic and piezoelectric sensors. Bulk processibility, nontoxicity and easy integration with Si-based integrated circuits are other advantages. Zinc oxide has existing industrial applications owing to its piezoelectric properties. Still the drawback of commercial ZnO LED devices is the failure to realize bipolar doping. Semiconductors devices used worldwide are all developed based on p-n junction. It is imperative that robust p-type ZnO can be produced for ZnO to become prominent manufactured semiconductor device.

Researchers found ZnO can achieve reproducible n-type doping with elements such as Al, Ga and F [14]. However reports of reproducible stable p-type ZnO have been highly contested. Initial 1st principle calculations determined that oxygen rich condition can produce p-type film [1]. Experimental attempts using group I and group V elements left researchers with optimism yet confusion. Past theoretical reports suggest group I elements such as Li, Na and K form the shallowest acceptor levels permissible for p-type conductivity. Experimentally, group I p-type

conduction could not be achieved due to self-compensation by intrinsic donor point defects. Similarly, this was observed in theoretical calculations and experimental attempts to doping ZnO with group V elements. Elements such as N, As and P were suggested as essential anionic substitutes to Oxygen. However, group V elements create deep defect levels and formation of compensating antisites defects due to orbital p-d repulsion. Nitrogen in particular created considerable attention being the only group V elements to form shallow acceptor level with small lattice distortion. A multitude of reports of p-type conduction are available. The limiting drawback for nitrogen reproducibility is its inherent low solubility in ZnO. With a decline in investigations due to lack of reliability of p-type ZnO a novel approach in recent years suggested Zn substitution for group 1B transition metals could overcome limitations found in group 1 and group V elements.

Recent 1st principle studies suggested that group-IB transition metals Cu, Ag and Au may substitute for Zn cations allowing p-type conduction [1]. Cu,Ag and Au are predicted to have transitional energies ε(0/-) 0.7,0.4 and 0.5 eV respectively making them candidates for shallow hole acceptors. The calculated formation energies are low for subsitutional sites but high for interstitial sites where hole compensation occurs. Under oxygen rich conditions which can suppress Vo compensation Cu,Ag and Au can produce p-type ZnO. Experimentally, It was confirmed by [2] that p-type ZnO can be achieved by pulsed laser deposition with Ag doped ZnO target with films grown at temperature above 200^{0}C with oxygen pressure of 3.5x10^{-1} Torr.

However, low hole mobility of 0.2-2.32 cm^{2}V s and high hole concentration of 4.9 x 10^{16}-6.0 x10^{17} cm^{-3} raise concern about reproducibility and low resistivity. Theoretical framework elucidating the possibility of group 1B elements substitution with Zn creates a dual

solution to small atomic radii and self-compensation of group I elements and high lattice distortion with group V elements with substitution with Zn. With little experimental validation on Au doping of ZnO it is the motivation of this investigation to realize the impurity effects of Au-doped ZnO by analysis of film morphology and change in physical properties. Pulsed laser deposition was used to deposit Au-ZnO films resulting in two phase Au-ZnO structure supported by microstructural analysis and film characterization.

Chapter 2 Literature Review

2.1 Advances in Oxide Semiconductors

Development and wide use of ceramic materials in electronics and packaging can be attributed to ceramics wide range of electrical conductivity, mechanical and thermal properties. In recent year the emphasis to realize thin electroceramic films has generated interests into oxide films. Oxides have outstanding physical properties with tunable conductivity ranging 25 orders of magnitude. “Numerous investigations of insulating oxides such as BeO, MgO and SiO_2 paved the way for large microelectronic integration and capacitor devices”. [3] Insulators serve as the separation medium for conductors in devices such as MOSFET(metal oxide field transistor effect) improving computing efficiency of integrated circuits with increased heat dissipation and mechanical support for smart devices. Playing a pivotal role in the information and technological age of the 21^{st} century; oxide film fabrication has provided applications in TCO(transparent conducting oxide), spintronics, semiconductor light sources and solar cells. Wide band gap semiconductors allow for high power devices, UV light sources and high temperature operation. Although, TCO ITO(indium tin oxide) has the lowest bulk resistivity of $1x\ 10^{-4}\Omega$ its material toxicity and raw material scarcity pushed efforts towards ZnO with comparable physical and electrical properties.

2.2 Zinc Oxide use in Transparent Conducting Oxides (TCO) and Spintronics

2.2.1 Transparent conducting oxides

Since the incorporation of silicon wafers in microelectronic devices in the 1960’s and 1970’s semiconductor materials have gained enormous interests for various device applications worldwide. Specifically compound semiconductor ZnO has gained substantial interests in the

research community in part because of its large exciton binding energy (60 meV) which could lead to lasing action based on exciton recombination even above room temperature. [4] Over the decades, ZnO semiconductor materials have demonstrated unique, reliable and robust properties. Owing to wide band gap of 3.3 eV at room temperature in the UV wavelength emission range, researchers have demonstrated that ZnO has many advantages over conventional TCO (transparent conducting oxide) ITO(indium tin oxide).

Zinc and tin oxides were demonstrated to [4] have similar optical and electrical properties, with different chemistry and zinc oxide being a reliable candidate for solar cells. It was shown that ZnO is little affected by hydrogen plasma but quite unstable in acids. Hydrogen plasma stability is important for processing of commercial solar cell modules; which ZnO serves as the TCO front contact for effective coupling of light into solar cell by refractive index matching. [5] Post deposition of surface textured ZnO:Al surface resulted in higher quantum efficiency than tin oxides as well as solar cell damp tests revealed that after 1000h ZnO:Al/Si/ZnO Ag nonencapsulated thin films were still stable [6]. ZnO multilayered films using a metal embedded layer have increased reliability for optoelectronic applications. ZnO/Ag/ZnO multilayer films with a 12 nm carrier injection midlayer gave suitable conductivity and transmittance in the UV-infrared range for optoelectronic devices on flexible polymeric substrates [7].Complementary investigation to reduce sheet resistance and increase carrier mobility without the loss of transparency were detailed in ZnO/Cu/ZnO multilayers with high conductivity dielectric-metal-dielectric films. The carrier concentration was reported to be $1.2x10^{22}$ cm^{-3}, with a resistivity of 6.9×10^{-5} Ωcm a transmittance above 80% at optimum copper layer thickness of 2-3 nm. Pulsed laser deposition was used to deposit Al -doped ZnO [8]. Average transmittance was found to be in a range of 86%-92% with resistivity 7.0×10^{-3} Ωcm in

high oxygen pressure environments. Lowest resistivity was found at $1.4x10^{-4}\Omega cm$ at 300℃ with 0.1 Torr oxygen pressure. This can be attributed to the fact that 1m Torr oxygen provides sufficient oxygen vacancies for low resistivity while decreasing transmittance [8].

2.2.2 Spintronics

Spintronics offer advantages to electron transport based devices owing to their capabilities to use both the spin and charge of electron [5]. As electronic based devices are reaching the quantum limit and approaching limitations of device scattering and heat dissipation; spintronics long coherence of spin moments provide promise of device efficiency and longevity. Fast, low power consuming devices could be achieved since flipping the spin takes 10-50 times less power and is ten times faster than transporting an electron through a MOSFET channel [5]. Potential applications for ferromagnetic semiconductors and oxides include electrically controlled magnetic sensors and actuators, high density ultra-low-power memory and logic, spin polarized light emitters for optical encoding, and advanced optical switches and modulators and devices with integrated magnetic, electronic and optical functionality [5].

DMS (diluted magnetic semiconductors) magnetically doped semiconductor. ZnO was reported to be magnetic when doped into Mn, Ni or Co. Mn has attracted a lot of attention for having spintronic potential when doped with ZnO having a Curie temperature of 300K relating to magnetic moments alignment. The controversy of whether the origins of magnetic behavior result from formation of magnetic cluster atoms in the host lattice or transition metal ion substitution causes free carrier mediation producing long range magnetic moments due to spin-spin coupling, remained a impeding issue. Experimental studies on the microstructural and magnetotransport properties of ZnO Mn DMS thin films showed high quality free dopant clustered films indicated strong sp-d exchange in ZnO DMS suggesting ferromagnetism does

not result from impurity precipitates [9] . DMS nanocrystals were produced to serve as building blocks to form ferromagnetic semiconductor structures of higher dimensionality [10]. Films were prepared using spin coated-nickel doped zinc oxide nanocrystalline thin films with high quality colloiodal DMS quantum dots as solution precursors, showed ferromagnetic behavior at Curie temperatures above 300 and 350K with saturation moments showing up to 0.1 Bohr magnetrons for nickel. A study considering the effect of dopant concentration on magnetism showed solubility limit of Mn into ZnO of 13% was exceeded by film deposition by PLD with more than 35% of Mn obtained resulting in increase in lattice constants. Over saturation of Mn content resulted in net saturated magnetizations of Mn^{+2} ions having small electron spin with spin glass behavior from cooled field characterization related to structures of secondary phases [5]. The paradigm and capabilities of ZnO for spintronic provide motivation for device fabrication for ZnO DMS. In order to realize various ZnO devices, asymmetric doping involving p-type conduction must be found.

2.3 Asymmetric Doping of ZnO

2.3.1 1st principle theoretical calculations of compensating for native point defects

Understanding the behavior of native point defects is essential to the successful application of any semiconductor. These defects often control, directly or indirectly, doping, compensation, minority carrier lifetime, and luminescence efficiency. They also assist the diffusion mechanisms involved in growth, processing and device degradation [11]. It is crucial to understand the formation energy and migration energy of intrinsic defects that influence semiconductor conductivity. “Today, integrated circuit microelectronic devices found in our computers, calculators and home appliances function because of highly controlled concentrations of specific impurities that are incorporated into small, localized regions of semiconducting

materials" [12].Common intrinsic point defect associated with ZnO and all materials are cation and anion vacancies, cation and anion interstitials and antisites which all play roles in mediation of impurity carriers within host lattice. The well-known p-type hole killer in ZnO are V_o oxygen vacancies and zinc interstitials Zn_i. As a result in resolving difficulties in p-type ZnO a multitude of theoretical methods have been employed for determining the presence of point defects.

Difficulties for p-type doping extends beyond zinc oxide, being a common issue related to wide band gap II-VI semiconductors. A theoretical investigation was done in 1995 emphasizing the effects of large atomic displacement [13]. This numerical model for large lattice relaxation identified low energy lattice instability responsible for acceptor passivation. First principal calculation showed that deep lattice defect complex DBB (Double Broken Bond) release free holes by two host broken bond creating anion-anion bond capturing extrinsic impurities and stabilized under large lattice distortion. Understanding how intrinsic defect formation causes lattice instability provided a beginning foundation to resolving unipolar doped ZnO. Numerical studies on the specific defect contribution was unknown until it was shown using high energy electron irradiation in zinc oxide producing shallow donors relating to Zn_i [14] . It was also suggested that production of defects was higher in Zn-face (0001) than O-face (0001) also that donors were found to be Zn_i even in non-irradiated samples.

1st principle pseudopotential method based on local density approximation (LDA) and density functional theory (DFT) were used to determine impurity defect formation energies, intrinsic point defect formation energies and defect complexes. A study using LDA investigating the effects of impurity compensation of p-type ZnO demonstrated that group I elements such as Li,Na,K have the shallow acceptor ionization (transition energies) meaning impurities can be ionized at 300K in this case for substitution of Zn atomic sites. Group V elements N, P and As

with the exception of N which have high ionization energies for substitution of O atomic sites of As_O 1.15 eV, P_O 0.93 eV and N_O 0.40 eV. Group I elements have with small perturbations to VBM due to reduced p-d coupling showing shallow levels for cation substitution. Ionization energies for group I elements were Li_{Zn} 0.09 eV, Na_{zn} 0.17eV and K_{zn} 0.32 eV respectively making them shallow acceptors relative to the Fermi level VBM (valence band maximum) [15] .

Previous studies have shown that impurity compensation can arise from the AX center instability from the double broken bond phenomenon. Modeled calculations explained that group V elements with the exception of Nitrogen have stable AX center while group I elements have metastable AX centers. Although group I elements have low ionization energies group I elements tend to occupy interstitial sites and become donors in the lattice when doped while their Fermi energy is close to VBM. Interstitials site formation energies for Li and Na are 1.58 eV and 0.87 eV which are more stable than substitutional sites. In regards to K, as the atomic radii increases Vo+Kzn deep acceptors are formed. Group V impurity complexes with the exception of N formed Zn antisites which are donor like compensators. Nitrogen has the lowest formation energy of defect complexes with 6.58 eV at the Fermi VBM. Calculated AX center destabilization demonstrated that P and As are metastable with negative stabilization energies of -0.46 eV and -0.18 eV owing to induced lattice strain by large atomic bond lengths and enhanced p-d coupling giving rise to deep impurity levels promoting compensation of introduces acceptors [15]. Nitrogen was suggested as the most preferable p-type impurity due to shallow acceptor level of 0.40 eV and comparable ionic radius of 0.183 nm to oxygen 0.163 nm.

2.3.2 Theoretical growth conditions and defect formation for N and P-type ZnO

Growth conditions play an important role for impurity incorporation and tailoring of electrical conductivity. The concentration of a point defect depends on its formation energy shown in Equation 1 below. Point defects with high formation energies will occur in low concentrations. It must also be noted that formation energy of a point defect is not constant but depends on growth or annealing conditions. Chemical potentials determine the relative abundance of Zn or O atoms. Charge influences defect formation and migration.

$$c = N_{\text{sites}} \exp\left(-\frac{E^f}{k_B T}\right)$$

Eq.1

It was found [18] by 1st principle calculations that ZnO is n-type in Zn rich conditions due to the presence of Zn_i supplying electrons at shallow levels and a low formation enthalpy in both oxygen rich and Zn rich conditions. Compensating O_i and zinc vacancies have high formation energies. Contrarily it is difficult to dope ZnO p-type in oxygen rich conditions since compensating hole killer defects Vo, Zn_i and Zn antistites have low enthalpy formation. The preceding suggests ZnO cannot be doped p type under thermal equilibrium. Recent substantial insight to theoretical framework used a corrected LDA +U model compared to previous employed models. The LDA+U illustrated that oxygen vacancies were not responsible for unintentional n-type doping and calculated accurate defect transition energy levels and defect temperature migration. It was concluded that Vo are deep donors and have high n-type formation energies. Background hydrogen impurities can substitute for oxygen site acting as shallow donor. Zinc vacancies have low formation energies under n-type also acting as green luminescence in

ZnO. Diffusion and migration barriers were seen to be higher for Vo, O_i and V_{zn} [17]. Defect transition energies dopant levels in host band gap for group I and group V elements were seen to be shallow level dopants. Defined as the Fermi level position where the formation energies of the same charge defect are equal. “If a defect transition level is positioned, such that defect can be ionized at room temperature, it is labeled a shallow level” [17]. It was also pointed out that the migration of point defects increase with temperature and are commonly associated with interstitials owing to high mobility and migration barrier for Zn_i and O_i of 0.57 eV and 1.1 eV respectively [17] .

2.4 Impurity attempts in p-type ZnO

2.4.1 Group I (Li, Na and K) elements

Dopants substituting at Zn cation site have been theoretically shown to produce the shallowest acceptor levels resulting in smaller perturbations of VBM than anion O sites. Group I elements such as Li, Na and K have a small mixing of p-d orbitals that reduce compensating defect complexes and deep defect levels. Mentioned previously, calculated shallow acceptor levels for Li, Na and K were 0.09 eV, 0.17 eV and 0.32 eV, which preferentially form shallow hole acceptors [15]. Experimental investigations of group I elements suggested p-type doping is possible ZnO: Li films grown by DC magnetron sputtering were reported for p-type via temperature dependent Hall measurements. PL measurements showed Li_{zn} acceptor activation energy of 110 +/- 10 meV as well as deep acceptor level at 250 meV corresponding to Li related complexes [18].

Na doped p-type film grown by PLD showed in order to produce Na_{zn} sites incorporation of H acting as mediator for mobility of Na_{zn} substitution allowed p-type conduction. However

the lack of hydrogen incorporation resulted in compensation of Na_i to Na_{zn} sites. It was seen that the solubility of Na_{zn} is not large enough to counteract the native donor defects as result Na doped ZnO have high resistivity. Shown in earlier 1st principle calculations of K large atomic mismatch produces lattice distortion and high defect complexes such as Kzn + Vo [17] . It was indicated that dissociation energy of 1.5eV for Li_{zn}-Li_i complex a stable can occur at 300°C [18].

2.4.2 Group V (N, Sb, P and As) and Group IV (Carbon) elements

Phosphorous and arsenic sources have been found to produce deep acceptor states. Since P is an anion substitute for O, the Po transition level has high ionization energy. Pseudopotentials calculations suggested that using a P_2O_5 sources in oxygen rich conditions will produce P_{zn}-$2V_{zn}$ complexes as acceptor levels [20]. A reported XPS spectrum of P doped p-type films grown on n-Si (100) substrate by MOCVD, illustrate phosphorous 2p peaks showing P-O bonds suggested P has substituted with Zn sites. However, P and all other Group V elements are anionic O acceptors which suggest the reactive acceptor defect is P_{zn}-$2V_{zn}$ complex. Arsenic and antimony like phosphorous have large atomic mismatch with O sites, theoretically it was shown that As_{zn}-$2V_{zn}$ complexes are formed with a shallow ionization energy of 0.15 eV [18] p-type ZnO:As films were prepared on GaAs substrates. XPS spectrum for As 3d signal referenced As-O peak at 42.6 eV suggesting that the As atom has not substituted with O atom but rather As_{zn}-$2V_{zn}$ complex acceptor. Low temperature PL measurements further suggested As acceptor complexes were the source of p-type doping with acceptor binding energy of 0.15 eV correlating to the theoretical transition energy calculations. A similar trend is seen with incorporation of antimony (Sb) p-type doped ZnO . The impurity size mismatch with O results of formation Sb_{zn}-

$2V_{zn}$ complexes supported by Sb-O bonds from Sb_{zn} substitution. Temperature dependent PL measurements showed acceptor activation energies of 0.14 and 0.15 eV [18].

Carbon was suggested as candidate for p-type behavior with $C_{zn}+2O_i$ acting as dominant acceptor. Unintentional p-type doped films MOCVD [20] showed hole concentration of 1.4 x 10^{17}-5.65 x 10^{18} cm^{-3} and acceptor activation energy of 50.2 meV. 1st principle studies of carbon with native point defect show in oxygen poor conditions Czn+ 2Oi are dominant acceptors suggesting ZnO can be doped p-type in oxygen rich growth conditions. Still little studies of theoretical and experimental merit support these claims.

Nitrogen doped ZnO

N-doped p-type ZnO underwent extensive investigations over the past 20 years. Owing to its shallow acceptor hole level 0.40 eV, metastable AX center and comparable ionic radius to oxygen. Various nitrogen sources were used to realize p-type conduction as well as attempts to co-dope ZnO with group III elements to enhance solubility.

Nitrogen gas sources such as N_2, NO, N_2O, NH_3 and Zn_3N_2 were used in vacuum deposition resulting in report of electrical properties, hole concentrations and hole mobility as well supporting surface analysis that imply sufficient solubility of nitrogen host source. An initial investigation revealed that the of N_2 and N_2/O_2 reactant sources produced films with high nitrogen incorporation and p-type conduction. Impurity depth profiling of nitrogen by SIMS (secondary ion mass spectroscopy) suggested that carrier concentration was ~$10^{19}cm^{-3}$ [19]. Molecular beam epitaxy (MBE) with radio frequency plasma source used O_2 and N_2 but was unable to produce p-type behavior. However N-doped films using a Li diffused seminsulating substrate using MBE by N_2 by revealed p-type behavior with a hole mobility of 2 $cm^2V^{-1}S^{-1}$ and

hole concentration of $9x10^{16}$ cm^{-3} complementary SIMS concentration of nitrogen grown sample two orders of magnitude higher than pristine ZnO substrates [19].Low temperature PL measurements revealed a peak near 3.32 eV due to neutral bound excitons with estimated acceptor level of 170 meV. Donor acceptor pair (DAP) transition calculations for acceptor pair energies ranging from 165-200 meV due to nitrogen doped samples by ion implantation which can be correlated DAP blueshifted transition in PL spectra from 20 meV-3.234 eV.

The use of ammonia NH_3 as active dopant source suggested that tailoring the concentration of ammonia with oxygen from 0-100% significantly alters the electrical behavior and point defect formation. Electrical properties were most improved at ammonia concentrations from 50-100% hole concentration and hole mobility were highest at 7.3 x 10^{17} cm^{-3} 1.3 cm^2 $V^{-1}S^{-1}$ with a resistivity of 31 Ωcm. Nitrogen is more suitable dopant, enhancing hole concentration. However, when ammonia is increased to 100% saturation the presence of Vo and Zn_i is increased due to the absence of oxygen for defect suppression resulting in polycrystalline film [19].

Co-doped p-type ZnO using Ga-N pairs via pulsed laser deposition (PLD) reportedly suppressed oxygen vacancy formation with the use of N_2O nitrogen source with Ga and N. Hall and Seebeck measurements confirmed electrical properties with a carrier concentration of 5 x 10^{19} cm^{-3} and mobility 0.07 cm^2 V^{-1} S^{-1}. Singh et al. however illustrated O_2 partial pressure dependency on p-type codoped Ga-N ZnO. As the oxygen partial pressure is increased over 50% the carrier changes from n-type to p-type. It was noted that continued increase in O_2 partial pressure decreases charge carrier mobility and increases resistivity suggesting that once sufficient interstitials and vacancy defects are suppressed over saturation will degrade crystal quality and decrease carrier transport and electrical behavior [19] .With extensive reports

involving nitrogen low solubility and hole mobility and poor stability, more efforts are needed for showing p-type doping for ZnO the impurity elements.

2.4.3 Group 1B (Cu, Ag and Au) elements

Ag doped ZnO

Experimentally it was confirmed that Ag was a successful dopant for p-type ZnO [2]. Structural and electrical characterization suggested that high c-axis orientation at 200^{o}C with single phase structure is responsible for high hole concentration of 6.0 x10^{17} cm^{-3} Optical properties by low temperature photoluminescence at 2K reported neutral bound exciton emitted at 3.317ev in Ag doped film 200^{o}C.

Copper

Copper has been noted to be responsible for the observed green luminescence in doped ZnO PL measurements. Cu also exhibits bipolar conduction behavior shown theoretically to produce p-type ZnO with Cu_2O in oxygen rich conditions and n-type conduction in ZnO deposited films. Calculated intrinsic defect formation energies and carrier concentration using Cu2O by [20] showed Cu_2O can achieve p-type conduction with suppression of hole compensators Vo and Zn_i. Zn rich conditions and O poor conditions were shown to stabilize hole defect with low enthalphy formation of V_{cu} sites and high enthalpy formation of Vo and Cu_i. The carrier concentrations of Cu-doped ZnO films Vo and Cu_i were observed to be lower in both cation and anionic rich conditions with increase of substrate temperature. However, experimental reports investigating the ferromagnetism of Cu doped ZnO [21] showed that Cu doped ZnO films grown on c-plane substrate by PLD showed Hall measurements of n-type conduction with

electron concentration of 3 x 10^{17} cm^{-3}. X-ray diffraction scans using both 2theta omega and phi scan showed highly crystalline c- axis alignment and hexagonal epitaxial symmetry with single phase ZnOCuO phase supported by Cu_{zn} substitution.

With theoretical and experimental investigations of p-type ZnO dating back over two decades, reproducible and stable p-type doping has yet to be realized. There are no known experimental reports on the use of Au-doped ZnO. This is the motivation of this research to investigate the growth of Au-doped ZnO for p-type conduction. Experimentally we investigate the growth of thin film morphology via pulsed laser deposition.

Chapter 3: Methods and Materials

3.1 Thin film growth by Pulsed Laser Deposition

Pulsed laser deposition (PLD) was used for growth of Au-doped ZnO. PLD is one of the most commonly used physical vapor techniques, the mechanics for film growth are described. A KrF excimer laser with UV wavelength of 248 nm was used to evaporate selected materials. In the PLD set up, an excimer laser is produced by chemical reaction of short lived dimeric KrF premix gas by an applied high voltage. After decomposition, the specific wavelength is released as a monocramatic beam. Premix laser pressure is held at 2350 Torr with the voltage source at 25 Kv [22]. The laser light is then focused through an adjustable focusing lens, which then passes through chamber window and onto ablation target. Vacuum base pressure for ablation can reach 10^{-6} Torr. During deposition, a maximum of six targets can be ablated in a rotating target carousel with optimized angle for uniform ablation. Ablation results in plasma plume being produced from the evaporated target, which is then expanded perpendicular. The condensation of the ablated species to the substrate surface, results in film growth.

The parameters influencing nucleation film growth are laser fluence, background pressure and substrate temperature. The substrate temperature can be adjusted from 23^{o}C-800^{o}C depending on preferred growth conditions. Depositions using background gas pressures can reach vacuum chamber pressures ranging from 10^{-5}-10^{-1} Torr. Laser fluence is determined by calculating the laser energy density. Laser paper with square grid geometry is placed on target carousel. Once the laser absorbing paper is placed inside chamber the paper is ablated with a few pulses usually 1-5 pulses to form a image of the laser. The spot size is then measured to determine its area [22].To account for the loss of energy during laser transmission a photodetector

is used to measure change in energy from laser chamber aperture. The change in energy is divided by spot size area for energy density as shown in Equation 2.The film growth rate is measured by doing step deposition by masking the specified substrate and choosing the appropriate target. After deposition is completed step size height is measured by profilometer to determine the growth rate. A photograph of PLD is shown below in Figure 1.

$$\text{Energy Density} = \frac{Laser\ Energy\ Joule(j)}{Area\ Spot\ Size\ (cm^2)} \quad \text{Eq.2}$$

Before samples are loaded into the PLD chamber, the vacuum chamber is thoroughly cleaned with acetone. The substrate holder oring for sealing the chamber is cleaned with deionized water to prevent degradation of the polymer seal. The substrate holder is then sand with coarse sand paper 240/280 grit to remove residual plume species surrounding the substrate from previous depositions. The substrate holder is then cleaned with acetone. Substrates prior to mounting on holder are prepared by ultrasonication with acetone, methanol, iso-prpopanol and deionized water for 5 minutes each to thoroughly clean substrates. Substrates are mounted on substrate holder by holder clip or silver paint for adhesion. To ensure plume alignment, the targets are pumped separately with holder up to 10^{-5} Torr by in series mechanical turbo pump and the ablated with over 2000 pulses to form plume spot size striation. The bottom chamber is sealed by closing gate valve top vacuum chamber and vented back to atmosphere. The substrate is mounted in middle of plume striation and repumped for film growth up base pressure of 10^{-6} Torr. Prior to deposition targets are preablated to ensure uniformity of condensing species. Substrate used were c-plane sapphire [0001] 5mm x5mm square dimensions with target substrate distance of 5cm. Pristine Gold and ZnO cylindrical targets are alternate ablated in varying temperature from 23^{0}C-700^{0}C with background gas pressure of mixed oxygen and nitrogen from

10^{-3} torr-10^{4} Torr.For samples grown at elevated temperature substrates are preheated 30 minutes prior to ablation, samples in the presence of oxygen and nitrogen are done after a base pressure of 10^{-6} Torr is reached. After base pressure is reached vacuum gate valve is closed to protect turbo pump and gases are introduced.

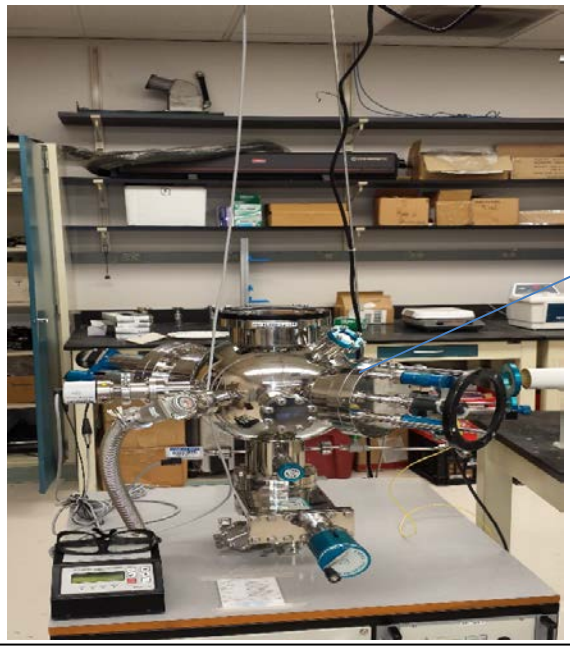

Figure 1. Photograph of pulsed laser deposition used for thin film growth

3.2 X-ray Photoelectron Spectroscopy

X-ray photoelectron spectroscopy (XPS) was used to analyze chemical composition, and oxidation states of various elements. XPS is done by placing samples in vacuum environment up to 10^{-9} Torr and transferred into an X-ray gun chamber. The samples are then irradiated by a monochromatic aluminum X-ray source with energy of 1486 eV 1 um depth penetration. During film surface irradiation, core or valence orbital electrons (photoelectrons) are excited with direct energy transfer. The excitation area is 10 mm-1 cm with electrons escaping from the top of 2-10 nm of the sample making it analytical surface sensitive technique. The ejected photoelectrons are deflected my stationary magnet inside chamber toward a collecting lens retarding photoelectron kinetic energy. Photoelectrons are then collected into a CCD spectrometer and peak signals are observed [23].

After photoelectrons are collected, the binding energy is measured with respect to intensity (arbitrary units relating to number of emitted photoelectrons in X-Y axis graph). Binding energy is energy required to remove an electron from a specific core or valence orbital and is measured by taking difference in incoming energy X-ray source and kinetic energy of ejected photoelectron described in Equation 3. By analyzing shifts in the binding energy with respect to intensity we can confirm composition and information about chemical environment. Semiquatification which determines elemental surface composition has error of $\pm$ 10%. The equation for elemental composition is described in Equation 4. Dividing a individual element orbital peak area by instrument sensitivity factor by summation of all peak areas and their respective sensitivity factor. A photograph of the XPS analysis chamber is shown in Figure 2. XPS instrument model used was Kratos AXIS 165 and Kratos Ultra Axis 165.

$$E_B = h\nu - KE \quad \text{Eq 3}$$

$$(\text{Atomic \%}) = \frac{peak\ area/asf}{\Sigma\ peak\ area/asf} \quad \text{Eq 4.}$$

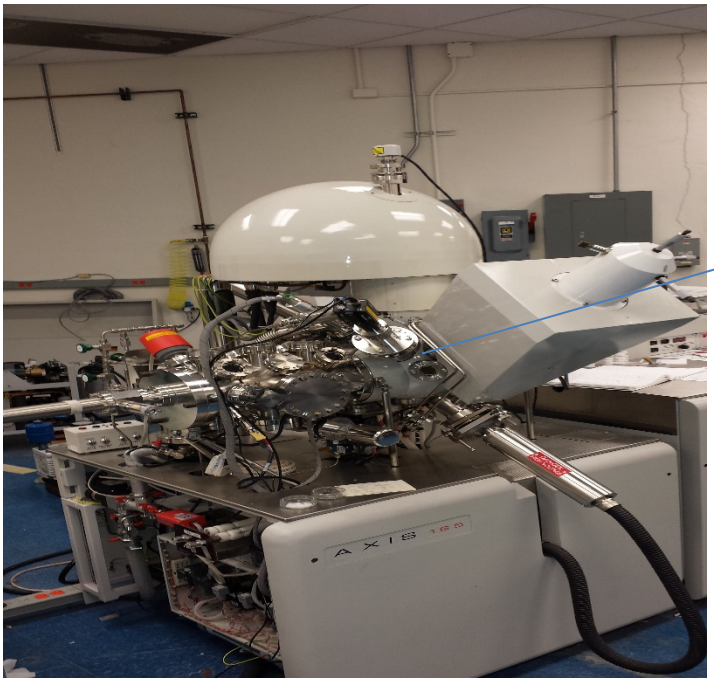

Figure 2. Photograph of XPS used for surface film chemical analysis

3.3 X-ray Diffraction

X-ray Diffraction (XRD) is a nondestructive technique that is used to determine phase structural information, grain size and lattice strain of substrate samples. Siemens/ Bruker D5000 2Θ/ω with Cu Kα radiation with an X-ray wavelength 0.15460 nm was employed to analyze substrate film crystallographic orientation. Diffraction follows the Bragg relationship to determine changes in lattice parameters with respect to incident angle intensity Θ shown in Equation 5. The number of reflections is equivalent to the angle at which incoming wavelengths constructively interfere with lattice spacing.

$$n\lambda = 2d\sin\theta \qquad \text{Eq 5.}$$

When sample are mounted the in diffraction chamber both λ and Θ are moving in 2ΘΩ scan with grain orientations perpendicular to the substrate surface providing peak intensity corresponding to elemental lattice planes. Grain size is calculated by using Scherrer equation shown in Equation 6. Scherrer equation is dependent on K grains shape factor 0.9 for spherical grains, full width half maximum intensity in radians for specified Bragg conditions. Lattice strain can be determined by measuring the difference in film lattice constant from bulk lattice constant divided by bulk constant seen in Equation 6. Changes in lattice strain provide information about the contraction and expansion of film lattice constant according to the substrate and growth parameters. Analyzing film lattice spacing with peak intensity, grain size and lattice strain morphology and sample crystal structure can be determined. A schematic of two theta omega scan using Braggs Law is shown below in Figure 3

$$\tau = \frac{K\lambda}{\beta\cos\theta} \qquad \text{Eq 6.}$$

$$E = \frac{\alpha\ meas - a\ bulk}{\alpha\ bulk} \qquad \text{Eq 7.}$$

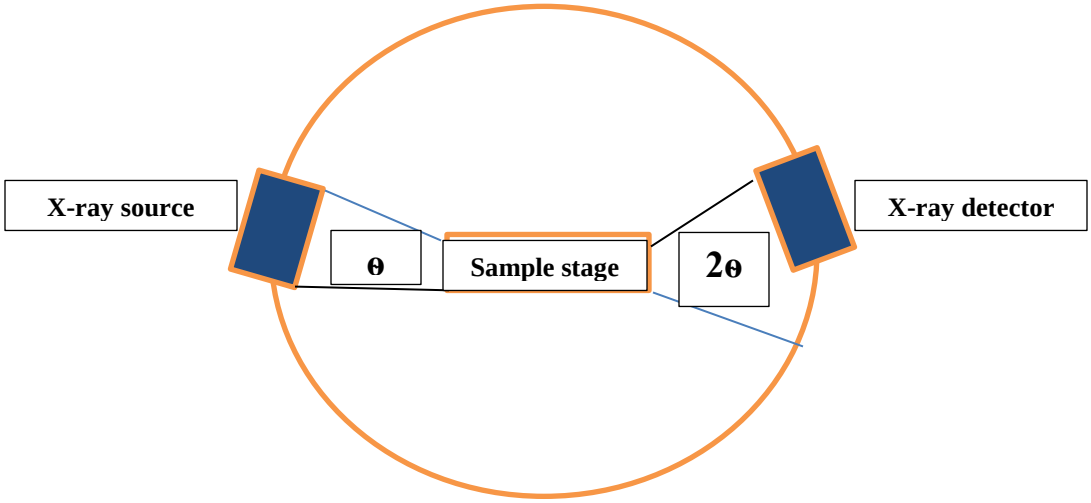

Figure 3. Illustration XRD 2ΘΩ standard scan using Braggs law for measuring diffracted peak intensities

3.4 Photoluminescence

Optical properties of films impurity defects were characterized by photoluminescence (PL). PL analysis is an nondestructive technique requiring little manipulation since the sample is optically excited. PL involves the spontaneous emission of fluorescent light sources ranging from 300 nm-800 nm from excitation light source of a different wavelength. Fluorescence (luminescence) is the result of electron hole recombination within sample material energy band gap. Temperature and excitation light source are crucial at probing impurity levels and energy band transitions. Excitation sources can use wavelengths ranging from UV-infrared and temperature which can be varied from 2 K-350 K.

Laser excitation source of 355 nm was used to probe sample with at temperatures at 300 K and 80 K for impurity levels defects and resolve non radiative recombination the result of electron-phonon coupling. Room temperature PL (300 K) is done by aligning laser optics and irradiating substrate. Low temperature luminescence at 80 K was done by placing samples in castor holder and pumping to vacuum of 10^{-4} Torr and cooled with liquid nitrogen to 80 K where optical transitions are observed. Typical PL set up is shown below in Figure 4 where variety of lenses and mirrors are used to reflect, refract laser beam towards sample with beam fluorescence aligned with a filter and spectrometer.

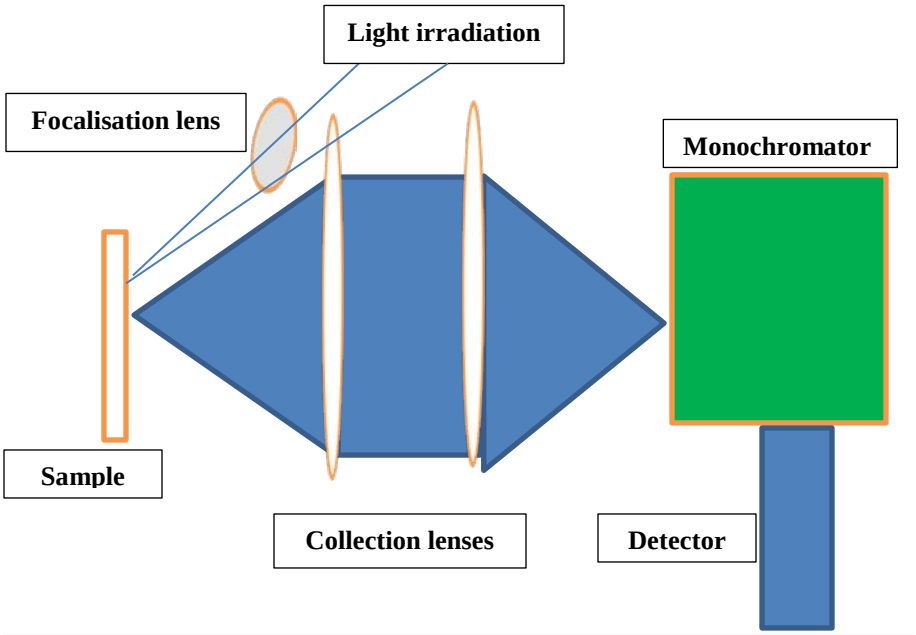

Figure 4. Illustration of PL apparatus for surface impurity defect analysis

3.5 Transmission Electron Microscopy

Microstructural information regarding film crystallinity and phase composition was done by transmission electron microscopy (TEM). TEM model used JEOL JEM 3010 analyze film by using electron beam gun at 300 kV. The electron beam is focused and aligned through a series of magnet lens and transmitted at the interface or cross section film and substrate film. A photograph of TEM apparatus is shown Figure 5. TEM imaging was followed by Electron Dispersive Spectroscopy (EDS) destructive analysis technique probing substrate film with high energetic electrons to determine films composition similar to XPS. Cross sectional TEM was used to analyze microstructural formation of grown films.

Figure 5. Photograph of TEM microstructural analysis

Chapter 4. Results and Discussion

4.1 Analysis of film composition

Film composition was determined by XPS quality scans on zinc, gold and oxygen orbitals. The Zn3p +Au4f and O 1s signals were calibrated with C 1s ranging from 282-286 eV with binding energies referenced to metallic Au to Au-O referenced by literature [23] and the NIST database. Deconvuluted Zn 3p+Au4f for the gold and zinc spectra, revealed surface bond formation of metallic gold and gold oxide molecules. Au-O bonds are first observed at room temperature with binding energy of 84.74 eV. The results suggest that the chemical environment resulted in two Au 4f peaks Au-O with Au^0 existed in films with increasing of substrate temperature during growth. The associated gold oxide and metallic gold binding energies are 85.63 eV and 83.97 eV. The formation of Au-O bonds shows Au has substituted for zinc creating Au+ions in Schottky defect. Standard metallic gold binding energies are found at 83.0-83.87 eV. The decrease in binding energy from 85.74 eV to 83.0 eV from oxide to metallic state shows more Au has diffused into ZnO with increasing temperature. This can be seen with higher metallic Au 4f intensities in all films grown above ambient conditions. The Zn 3p was resolved and referenced to ZnO at 88.0 in all growth conditions.

Figures 6-8 illustrate chemical shifts in Zn 3p + Au4f with metallic gold and gold oxide formation. Table 1 shows the calibrated orbital peaks and referenced literature [23]. The O1s was deconvuluted with two asymmetric peaks referenced to ZnO and AuO peaks at 530.18 eV and 530.30 eV respectively. A consistent FWHM (full width half maximum) separation of 1.0-2.0 eV, for all films is described in Figure 10, suggesting consistent change in the chemical environment. The chemical shift in the oxygen O1s peak for samples grown at room temperature

grown to 300°C, 500°C, 700°C O^{2}/N^{-3} background gas mix pressure is similar to the shift compared to those in Au-O to Au^{0} bond formation in the Zn3+Au4f peak. Figure 9 and Figure 11 demonstrate the formation of ZnO and Au-O in the O 1s signal with increasing film growth temperature

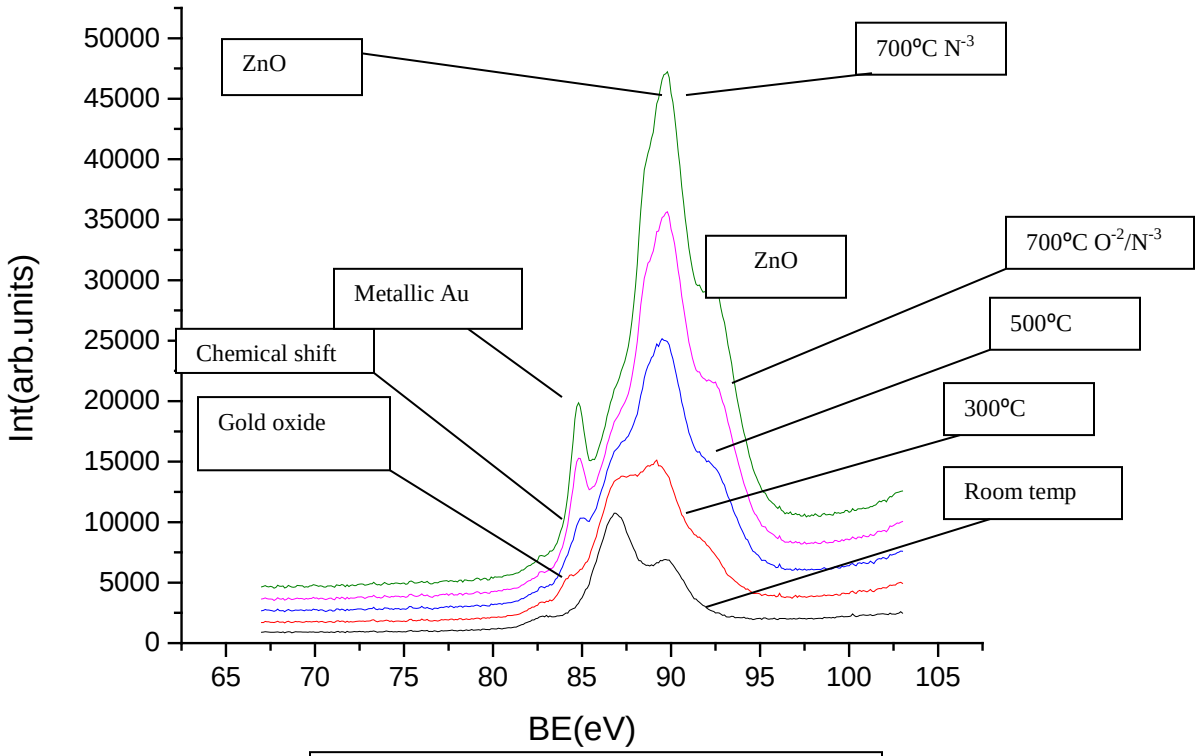

Figure 6. Zn3p+ Au4f BE Peak film comparison

Sample	Metallic Gold 7/2 & 5/2	Au-oxide 7/2 & 5/2	C 1s
RT 23°C		84.74/88.37	282.94
300°C	83.97/87.63	85.63/89.28	285.39
500°C	83.66/87.31	85.56/89.25	286.25
700°C Oxygen/Nitroger	83.52/87.18	85.69/89.47	286.22
700°C Nitrogen	83.51/87.15	85.73/89.44	286.35

Table 1. Zn3p+Au4f calibrated binding energies

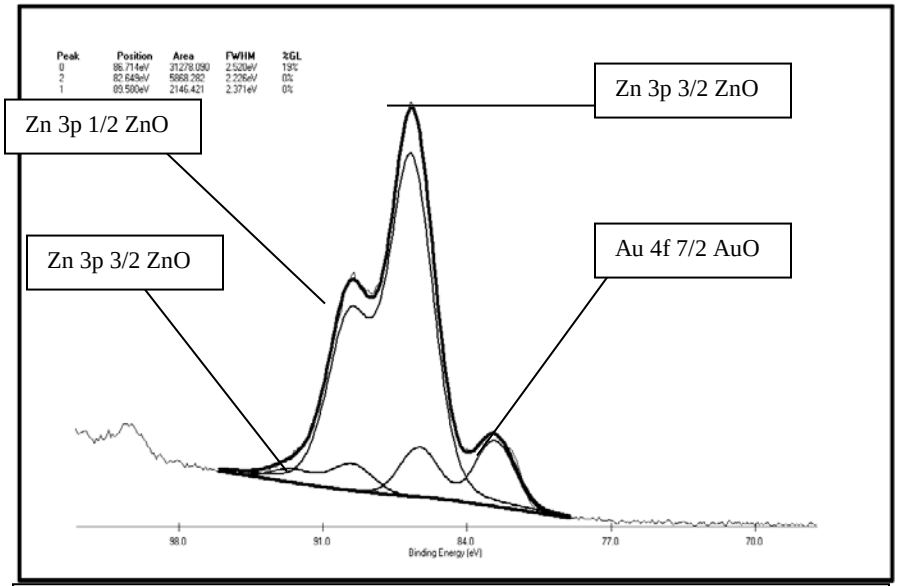

Figure 7. Au oxidation in Zn3p + Au4f signal at ambient growth conditions

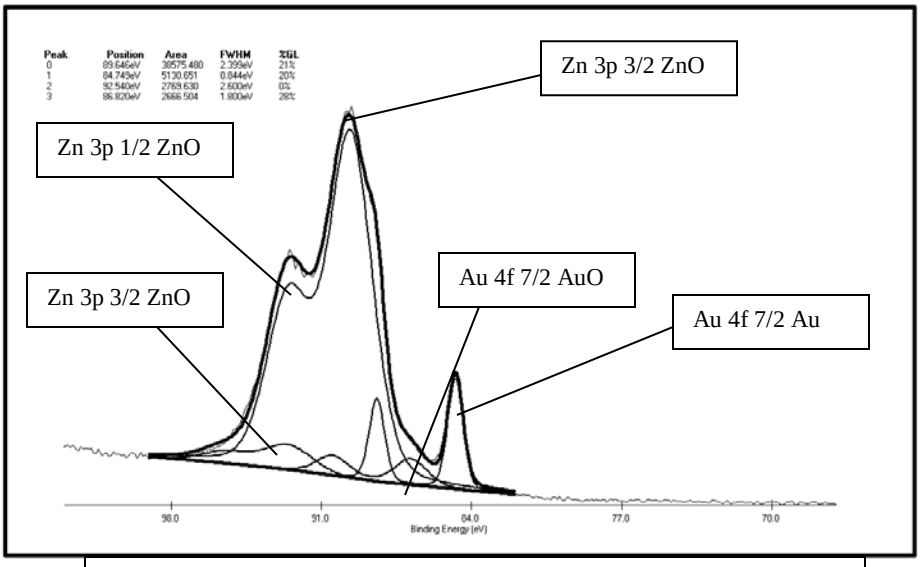

Figure 8. Zn3p + Au4f signal at 700°c O^{-2}/N^{-3} growth conditions

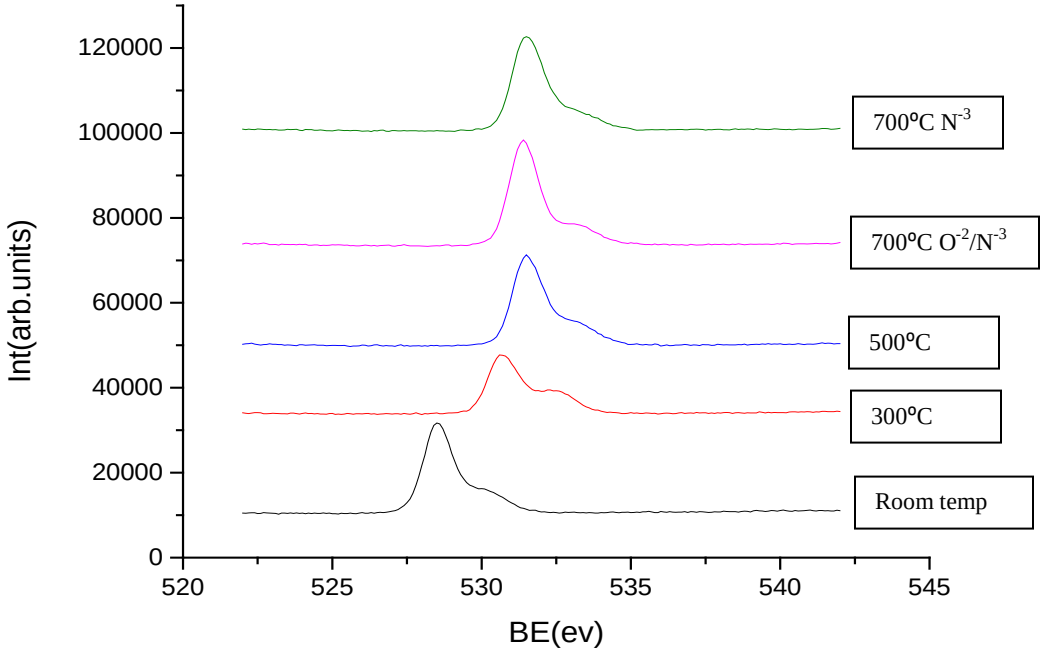

Figure 9. O 1s peak binding energy peak film overlay

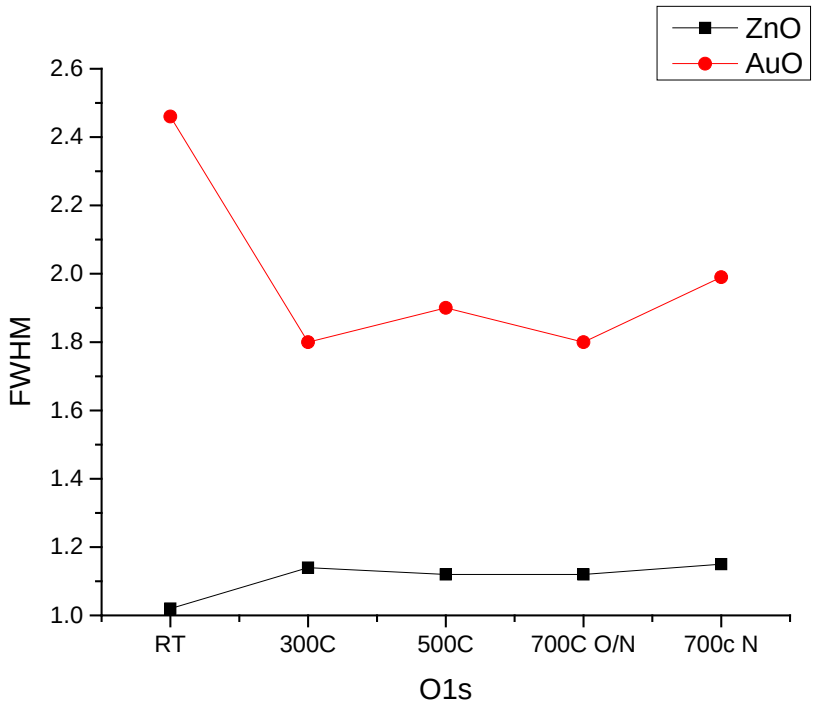

Figure 10. O1s FWHM evolution

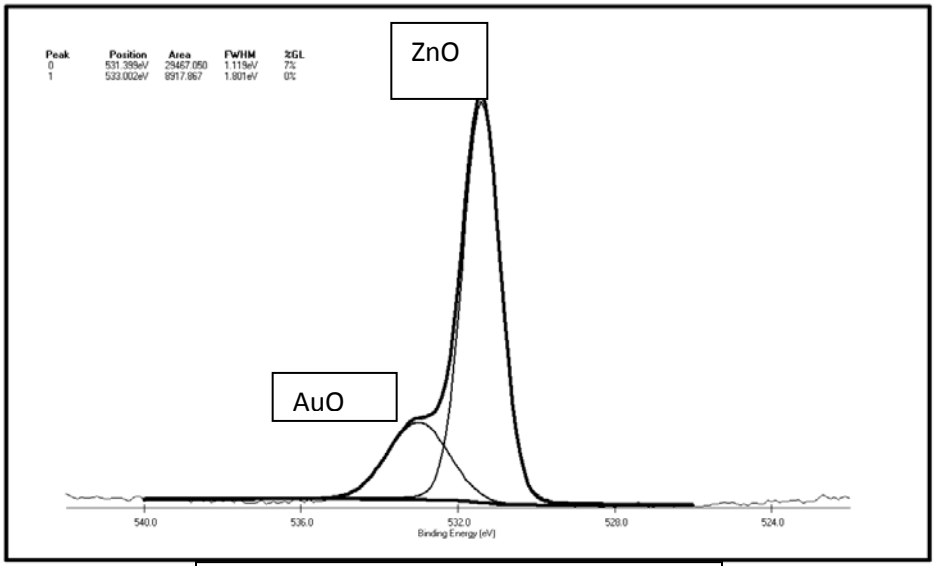

Figure 11. O 1s AuO and ZnO peak identification

4.2 Structural Properties of Multiphase Au-ZnO

Chemical bonding information from XPS was complemented with structural information provided by X-ray diffraction 2ΘΩ scan. Hexagonal ZnO [002] and cubic Au [111] peaks were indexed and c-plane sapphire substrate. ZnO and Au diffracted peaks suggested a formation multiphase film structure. Multiphase structure is shown to be temperature dependent. As the growth temperature is increased Au diffusion is increased and exceeds solute solubility limit resulting in the precipitation of the second phase. Elevating the temperature influences film crystallinity and lattice strain. Crystallinity is shown to temperature dependent in film gowth. High c-axis orientation intensity is observed 700ºC in a mixed oxygen/nitrogen environment Lattice c-strain is also inversely proportional to temperature with decrease in strain showing film compression to match sapphire lattice. The grain size is directly proportional with temperature with increasing grains from 9.6 nm to 23 nm with increased temperature from 23ºC- 700ºC. Figure 12 provides a peak overlay of all grown films lattice indexing with elemental composition.

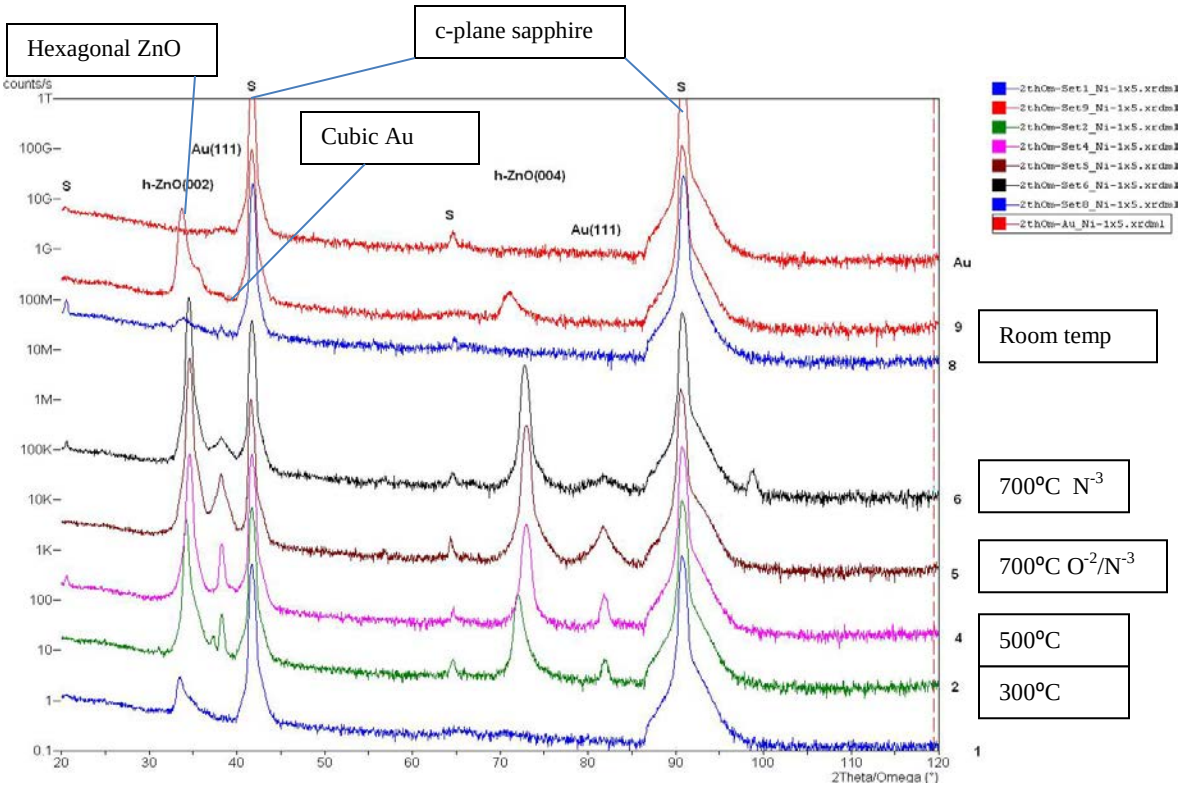

Figure 12. XRD peak overlay phase morphology c-plane [0001] substrate

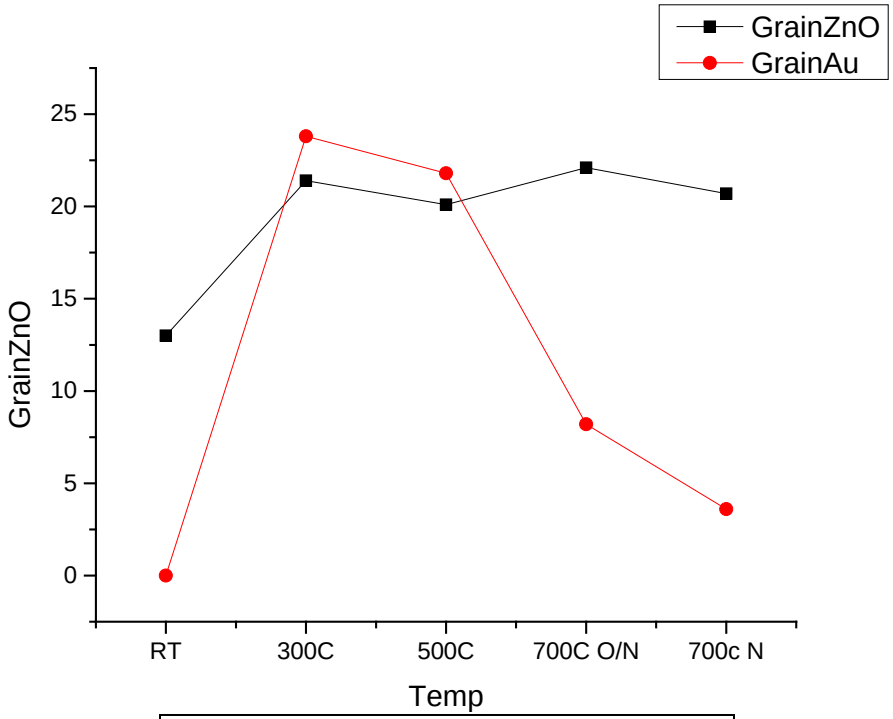

Figure 13 a-c. Evolution of grain size with

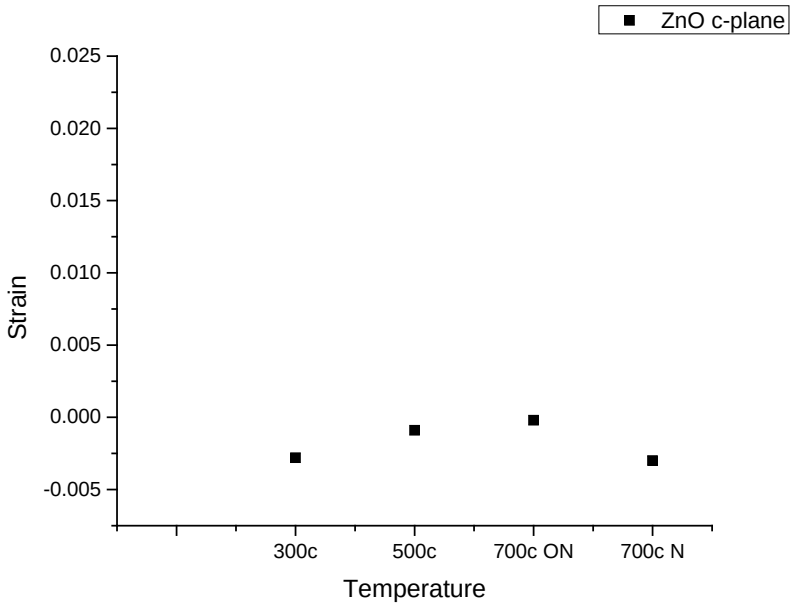

Figure 13 b. c-plane strain with temperature

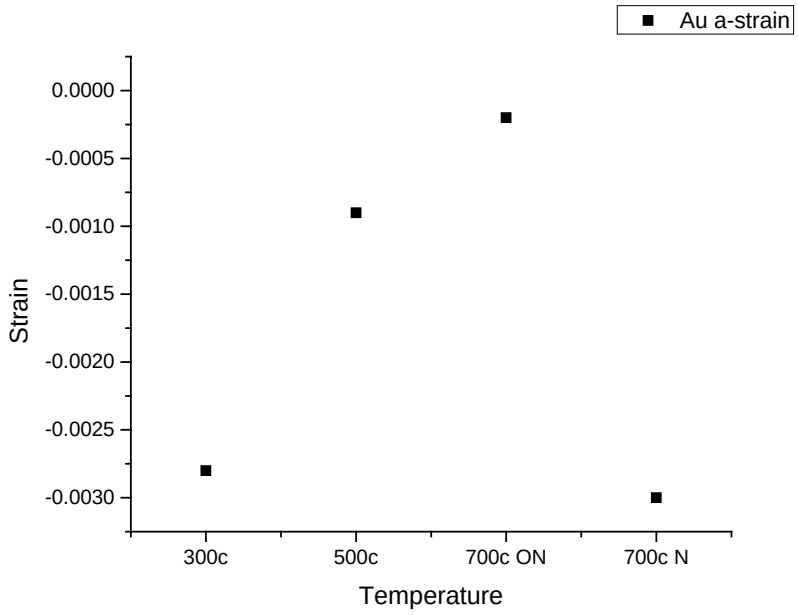

Figure 13 c. a-plane strain with temperature

The contraction and expansion of hexagonal zinc oxide and cubic Au lattice was observed. Expansion of lattice constant resulted in positive lattice strain, which is larger than bulk lattice constant for both ZnO and Au. Contraction of lattice constant resulted in negative lattice strain smaller than bulk lattice constants. Figure 13 provides film growth temperature versus strain relationship. Positive lattice strain was measured in films grown at room temperature while negative lattice strain was found in samples grown at high temperatures as shown in Table 2.

Sample	h-ZnO c-const	ZnO c-strain	Au cubic const	Au a-strain
RT	0.5323	0.03107	Peak too weak	Peak too weak
300◦ C	0.52486	0.00796	0.406	-0.0028
500° C	0.51818	-0.0048	0.407	-0.00091
700 °C O/N	0.5183	-0.0046	0.407	-0.00027
700° C N	0.5196	-0.0021	0.407	-0.00039

Table 2. Lattice expansion with temperature

4.3 Optical properties of impurity defect levels

Room temperature and low temperature photoluminescence measurements at 300 K and 80 K were used to identify impurity defects. Room temperature measurements on samples with increasing temperature showed broad blue band florescence corresponding to free electron to donor and donor acceptor pair transitions (DAP) at 380nm [25]. Growth conditions of 700°C with O^{-2}/N^{-3} partial pressure resulted from broad band flourescence with several shoulder peaks

shifting from blue band to green band emission from suggested DAP transitions coupled with phonon recombination with energy band gap. Flourescence peaks observed at 300ºC and 700ºC O^{-2}/N^{-3} are consistent with fluorescence intensities at 80 K shown in Figures 14-19.Low temperature fluorescence at 80 K for film growth at 300º C resulted in slight green band shift from 380 nm to 400 nm. Dominant defect impurity levels are described in peak overlay in Figures 19-20.

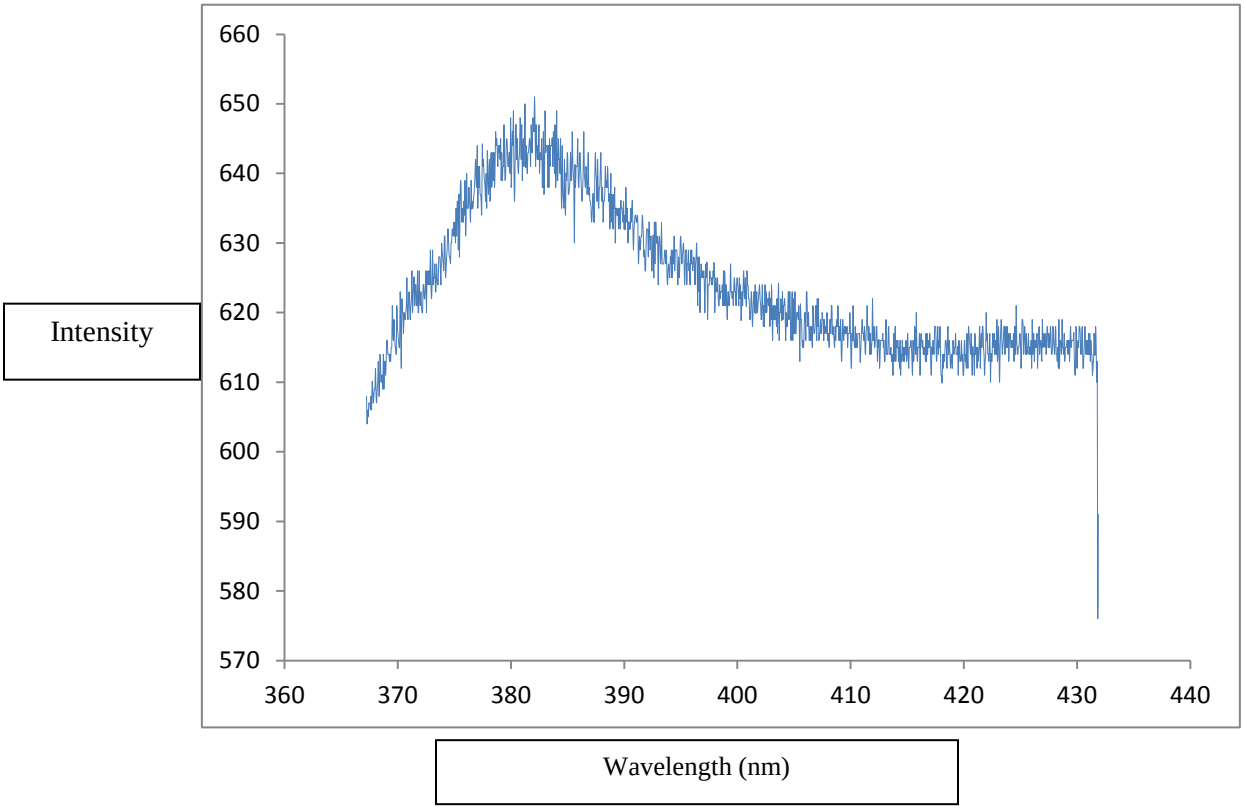

Figure 14. Film growth at 300ºC Room temp PL

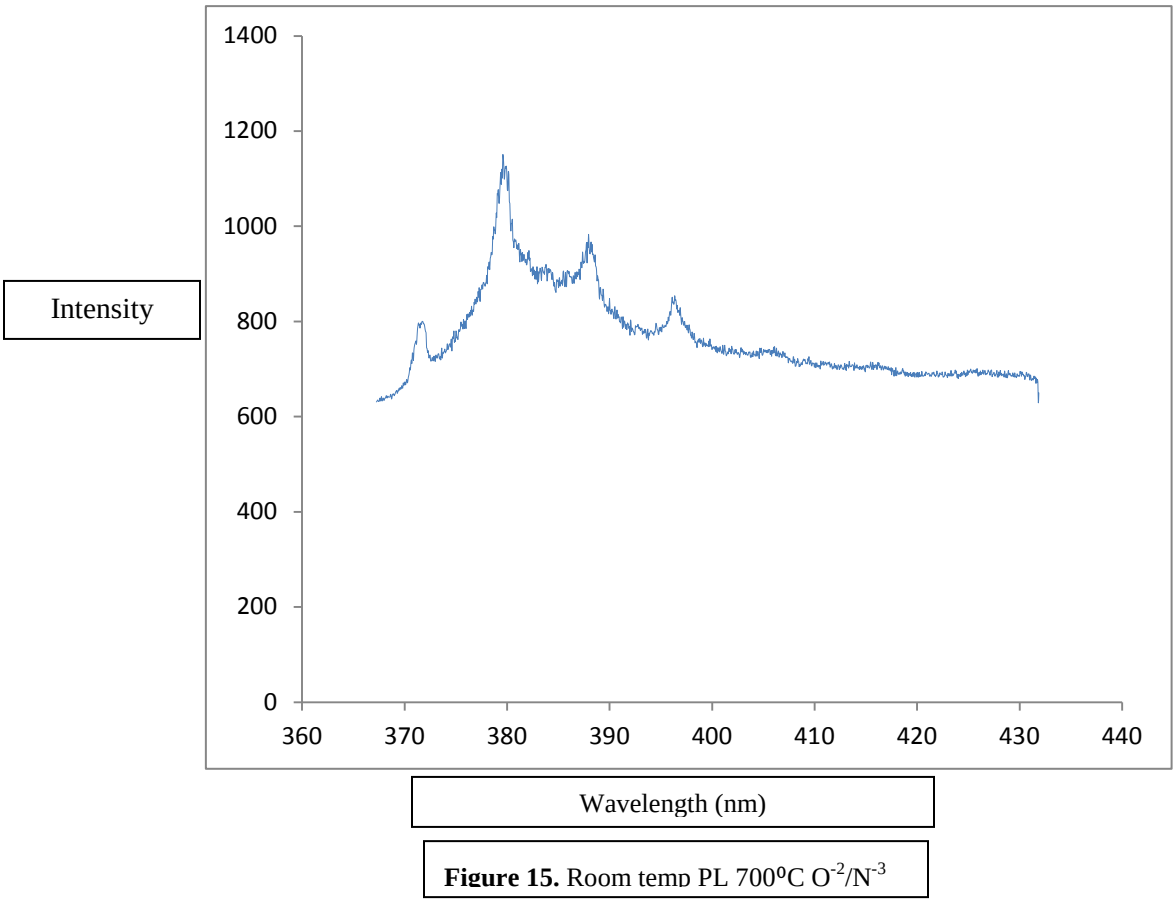

Figure 15. Room temp PL 700^{o}C O^{-2}/N^{-3}

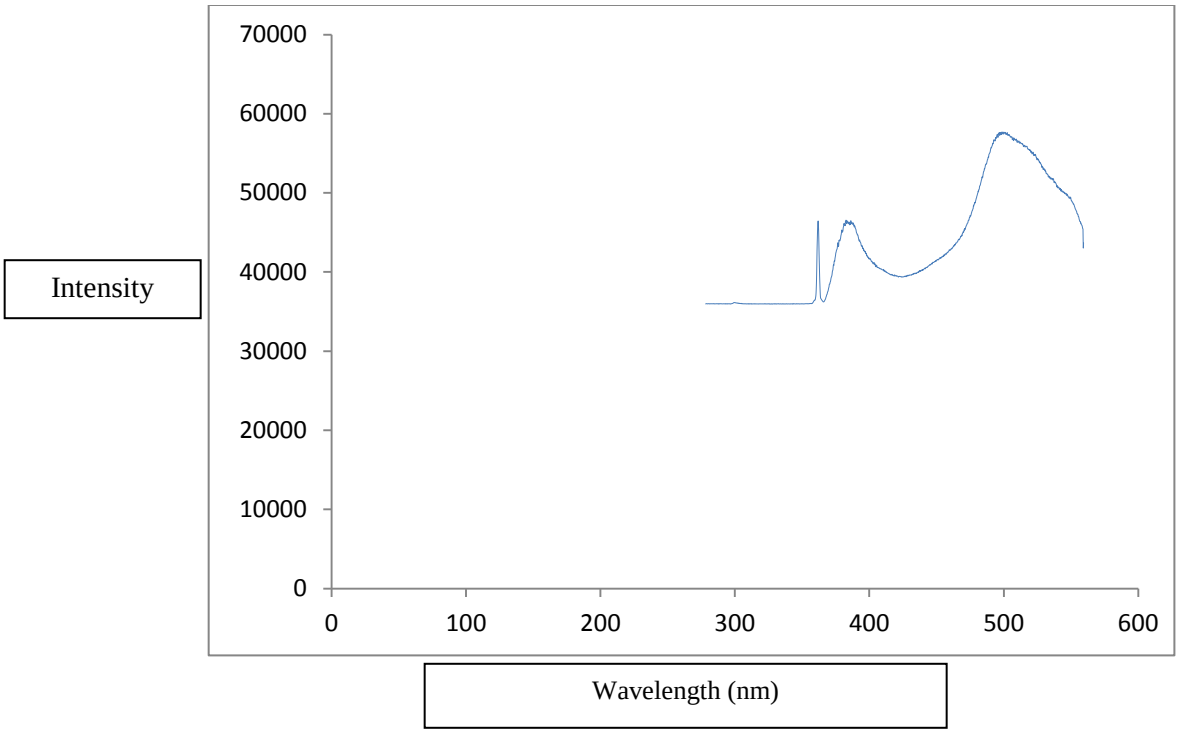

Figure 16. Low temp PL 300º C

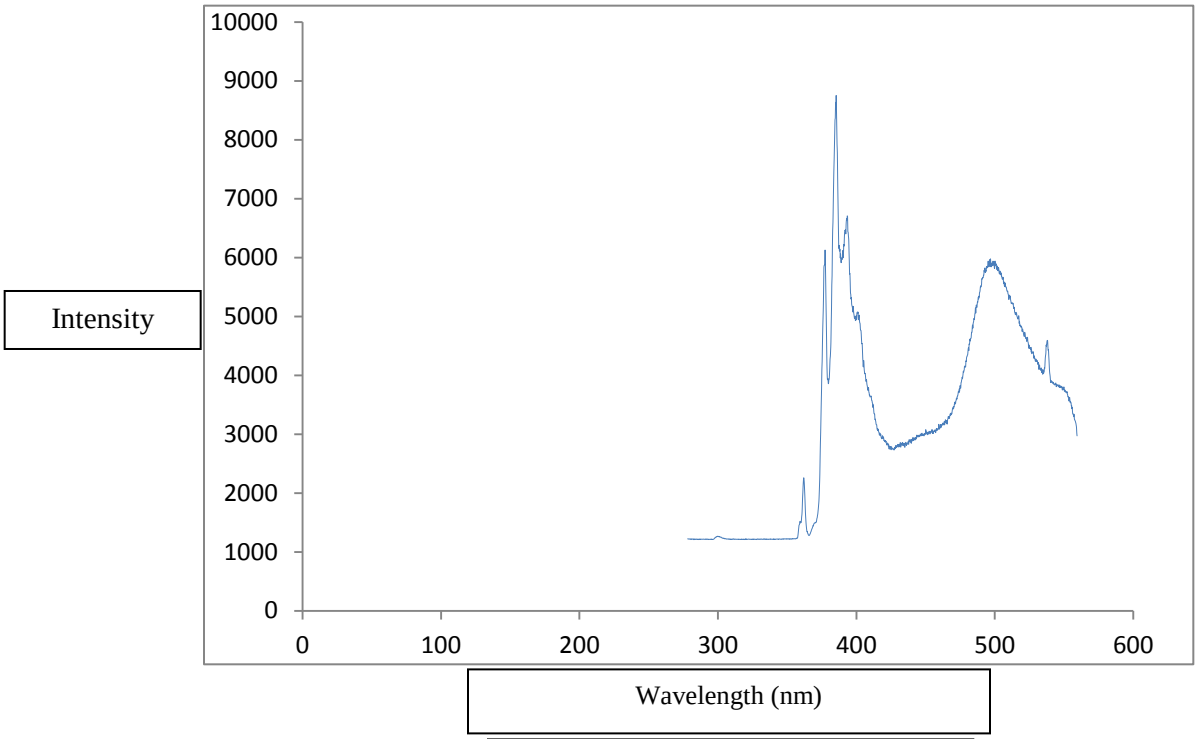

Figure 17. Low temp PL 700ºC O^{-2}/N^{-3}

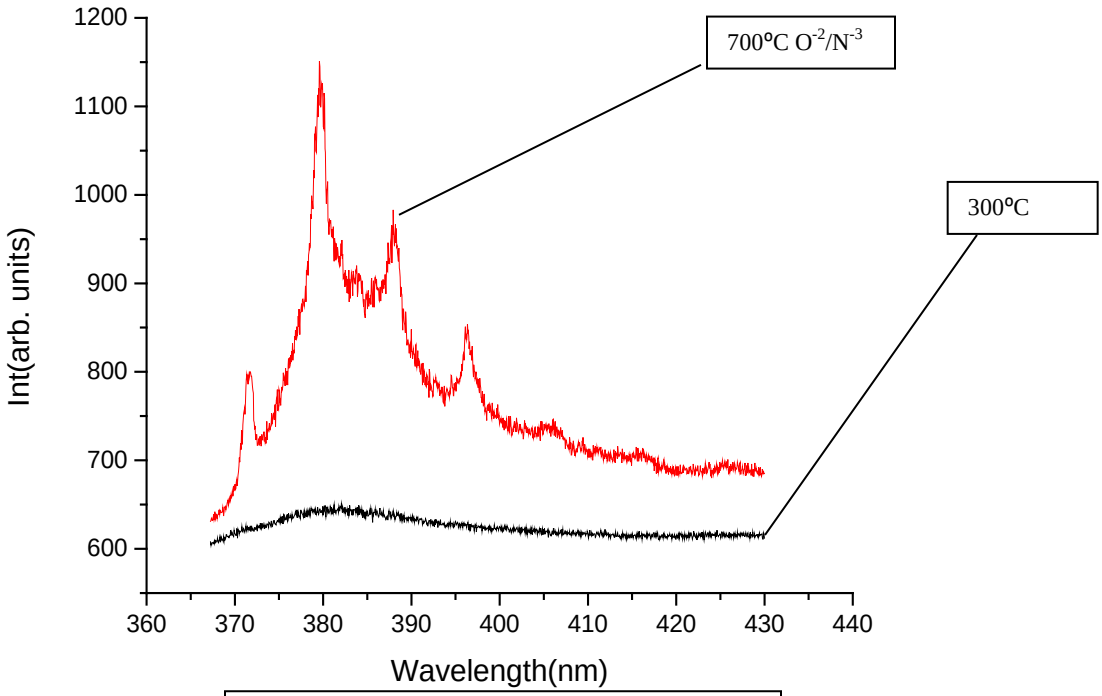

Figure 18. 300K PL peak film comparison

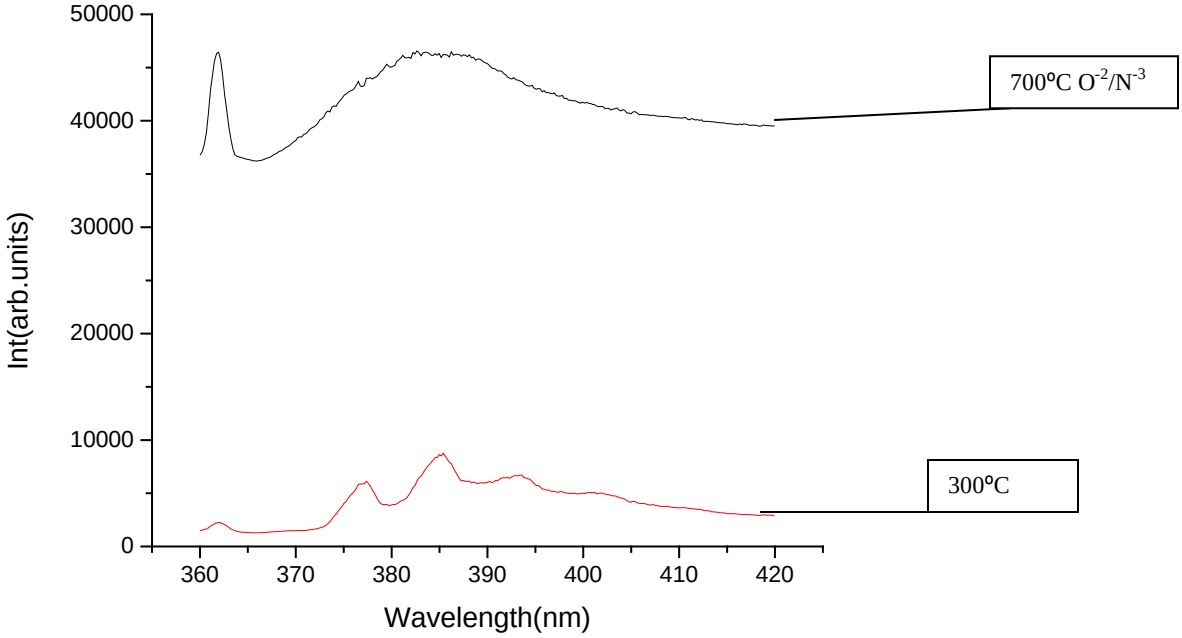

Figure 19. 80K PL peak film comparison

4.4 Microstructural morphology of Au-doped ZnO

Cross sectional TEM images show, crystalline orientation at Au-ZnO c-plane sapphire interface. Preliminary images suggest high crystalline orientation of ZnO (002) c-axis orientation Au (111) a-plane cubic phase is described in Figure 20. Structural defects are illustrated in formation of grain and phase boundaries caused by incorporation of Au in ZnO lattice shown in figures 21-22. Dark circular spots at different film locations shown in Figures 23-24 suggest the presence of Au precipitates previously noted to result multiphase structure formation by XRD and XPS structural and chemical analysis.

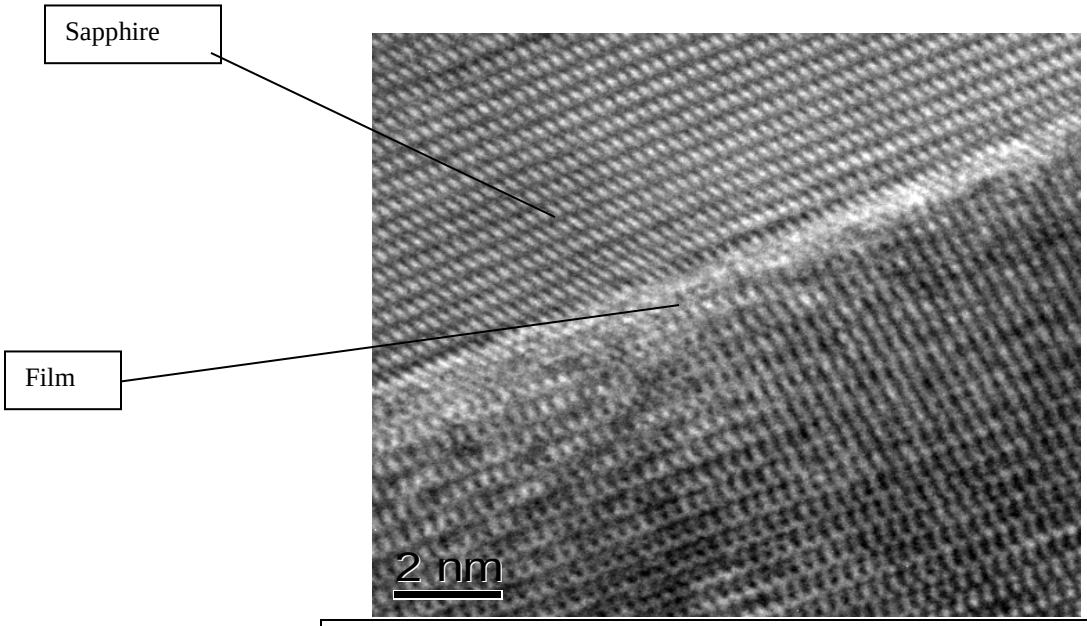

Figure 20. Film substrate interface illustrating high crystal orientation

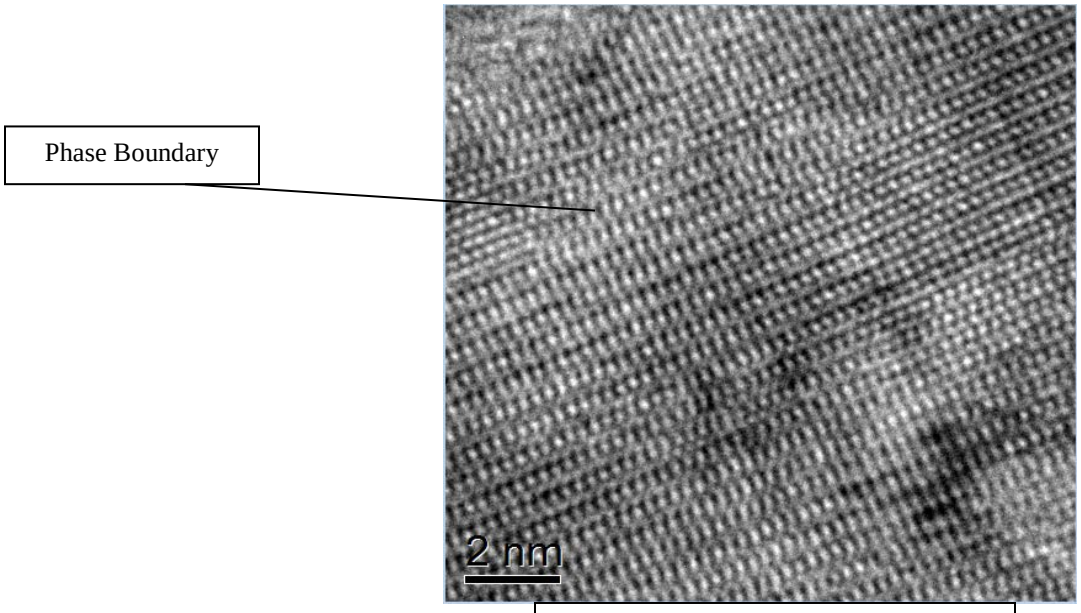

Figure 21. Multiphase boundary defect

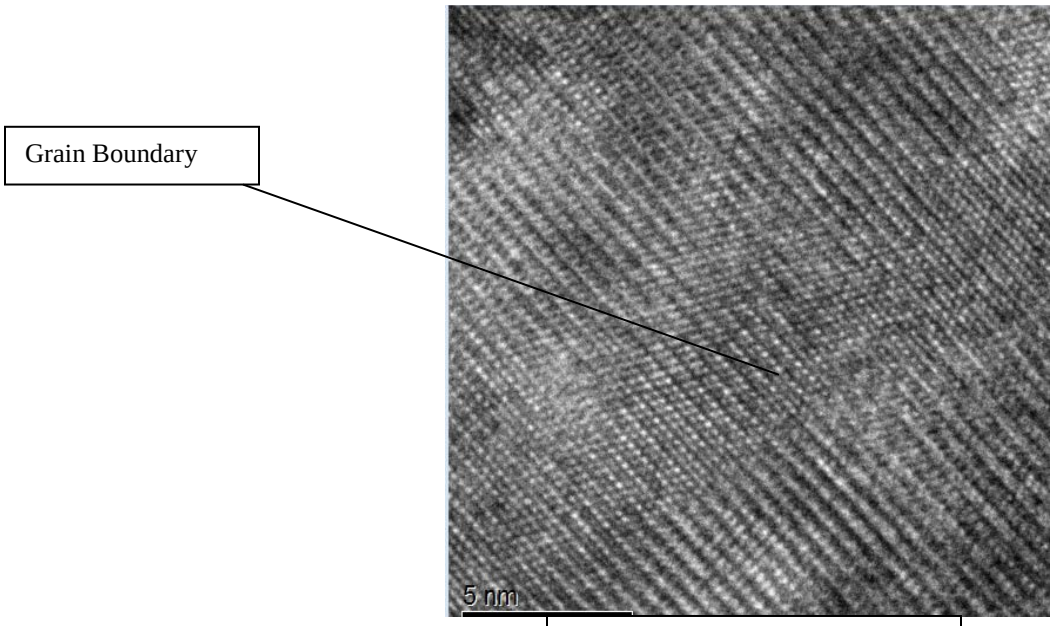

Figure 22. Grain boundary defect

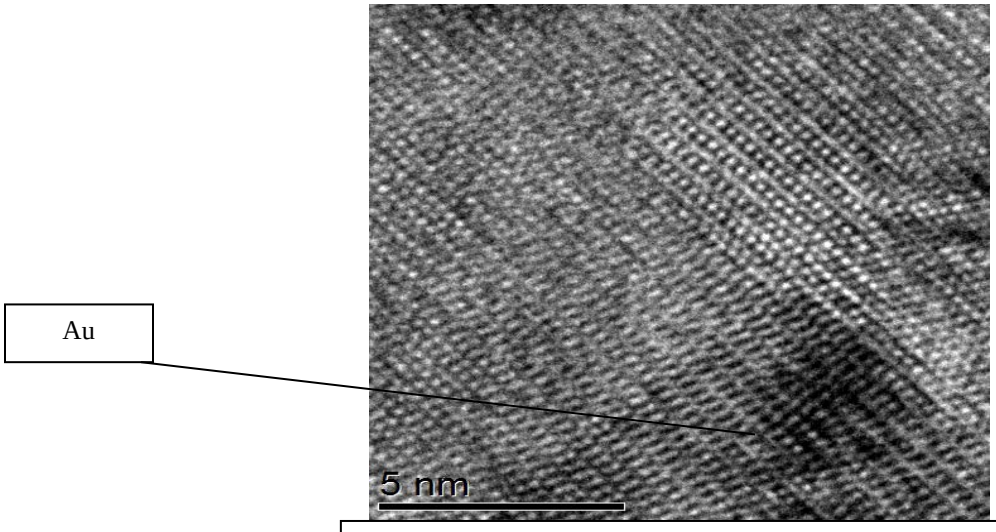

Figure 23. Au precipitation from multiphase film formation

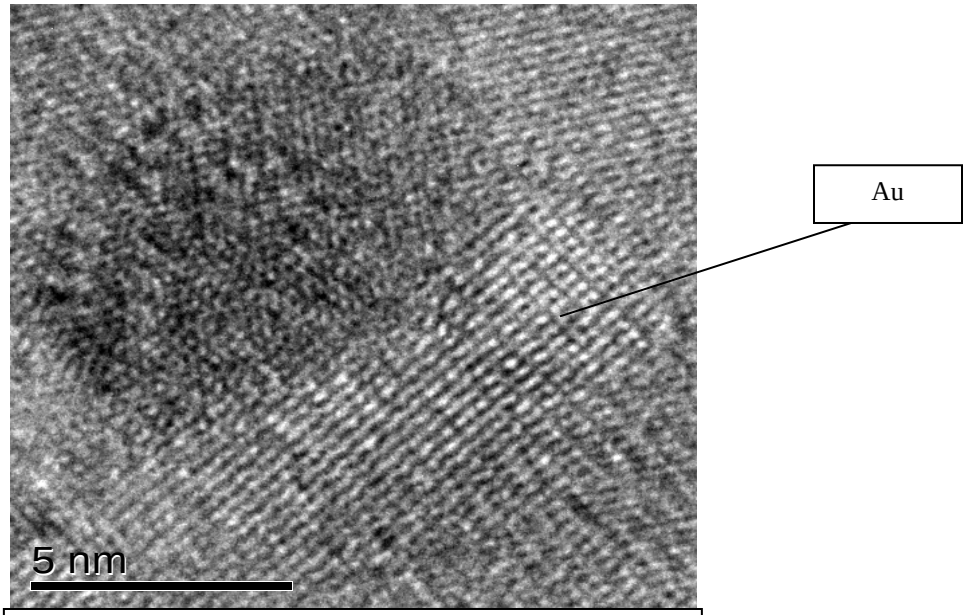

Figure 24. Au precipitation from multiphase film formation

Chapter 5: Conclusions

5.1 Morphology of film growth by PLD

Deposited Au-ZnO films on c-plane sapphire

Pulsed laser deposition was used to grow Au-doped ZnO thin films on c-plane sapphire substrates. ZnO and Au targets were alternately ablated with a fixed pulsed rate for each target with a frequency of 10 Hertz. Deposition kinetics of impurity diffusion was aided by external growth influences Film growth was affected by change in plume particle distribution by temperature and background gas. Films grown in elevated temperature from ambient conditions to 700^{0} C produced two phase Au-ZnO structure. Au diffusion was enhanced with increased substrate temperatures resulting in Au solute atoms exceeding the solubility limit forming a second metallic Au phase. Films grown in oxygen and nitrogen background pressures have a decreased rate of diffusion of Au into ZnO host lattice due to increase in Au plume spatial distribution and decrease in depositing particle mean free path. Strong c-axis hexagonal (002) orientation was observed with films grown at 700^{0}C.

5.2 Physical properties of Au-doped ZnO Thin films

Structural, Chemical and Optical Properties

Structural Properties

Structural property characterization by x-ray diffraction reported impurity saturated ZnO lattice resulted in formation of multiphase Au-ZnO heterogeneous structure. The transition from single phase to multiphase was observed in films grown at elevated temperatures. High dopant interdiffusion led to the excess of Au this can be seen in the presence of Au (111) peaks in films

grown from 300^{0} C-700^{0}C. Schottky defects validated formation of Au_{zn}(Au-zinc substitutional sites) defects . Films grown at temperatures exceeding the binary intermetallic phase formation of AuZn alloy at 300^{0}C were absent of AuZn diffracted peaks. Absence of AuZn diffracted peaks demonstrates Au has preferred cationic substitution supporting theoretical studies. Film crystallinity was observed with high c-axis orientation at 700^{0} C with mixed partial gas pressure. ZnO (002) high orientation can be explained by compressive lattice strain as film converges to substrate lattice. In addition to the increase in lattice of strain in both constituents; Au and ZnO grain sizes increased with temperature as well which can be related to enhanced nucleation and atomic coalescence promoting quality film growth.

Chemical and Optical Properties

Chemical surface bond analysis by XPS further realized Au_{zn} substitution in ZnO with formation of Au-O bonds by forming Schottky defects. Film growth at 760 Torr, elevated chamber gas pressures and temperature resulted emission photoelectrons related to Au-O bonding. This was evidenced by the Au 4f binding energy shifts of Zn3p+Au4f of 85.74 eV from standard metallic Au binding energies of 83.97 eV. The observed XRD multiphase diffraction peaks of Au (111) in films at elevated temperature growth was supported by bond formation of Au-O and metallic Au peaks. Deconvoluted Zn3p+Au 4f peaks resulted in two peaks, consisting of Au-O and metallic Au peaks and Zn 3p peak for ZnO at 88.0 eV. The FWHM broadening of the O 1s signal of two asymmetric peaks referenced to ZnO and Au-O at binding energy shifts of 530.30 eV and 530.18 eV respectively. O 1s full width half maximum was constant in all Au-O films with corresponding asymmetric peaks values of 1.13 and 1.80 relating to dominant Au-O formation throughout films growth conditions. The XPS peaks were calibrated by C 1s signal

and standard C 1s signal of 285.0 eV. Au-O bonds were referenced from literature [23] as well as standard XPS scan of Au and ZnO targets.

Optical properties

PL was used to probe impurity electron –hole recombinations, that originate from within ZnO band gap. Primary PL measurements revealed the presence of doped shallow and deep impurity defect levels. ZnO energy band was probed by of 355 nm excitation source revealing broad shoulder fluorescence observed in film growth at 300^{o}C while shallow impurity levels defects are suggested by multiple narrow shoulder peaks observed at 700^{o}C with O^{-2}/N^{-3} partial background gas pressures. It was found that non radiative recombination of lattice phonon electron-hole coupled luminescence was not the source of the multiple shoulder peaks, elucidated by of Raman scattering peaks that did not match the wavelength of the PL spectra. ZnO has energy band of 3.37 eV with fluorescence in blue range of 367 nm with a excitation source of 355 nm that probes more deeply that shallow levels which can explain the broad shoulder found at 300^{o}C. However, multiple shoulder peaks reported from [25] and [26] suggested that radiative recombination correlates to shallow impurity levels found in p-type films by acceptor bound and free acceptor excitons. Film growth in high pressure environments has been known to suppress the formation of hole killer oxygen vacancies that have green band luminescence, which dominates in undoped ZnO and n-type films. It is suggested that sufficient Vo are suppressed and have shallow impurity level defects explained by the observed increase in fluorescence at 300 K and decrease in fluorescence at 80 K at 700^{o}C O^{-2}/N^{-3}. However, the increased fluorescence at 80 K and decreased fluorescence at 300 K further suggests existing

deep impurity defects exist at 300^{0}C. Furthermore, the use of a 355 nm excitation source probes within band gap and excites more deep level defects. In both PL results done at 300 K and 80 K Au can be incorporated into ZnO with high solubility forming dominant energy band impurity levels.

Microstructural atomic arrangement

Cross sectional TEM images complemented XPS and XRD analysis results showing the existence of Au-O bonds and Au-ZnO multiphase structure. TEM images also suggest phase formation with ZnO (002) and Au (111) lattice spacing. Structural, chemical and optical analysis is supported by TEM cross sectional imaging. Interfacial defects consisting of grain and phase boundaries are observed. Grain boundary defects demonstrate the convergence of Au and ZnO crystal structure. Phase boundaries at the interface of the Au-ZnO alloy and multiphase structure are observed, supporting negative and positive strain found in the ZnO and Au lattice by XRD.. Isolated dark spot in the images are believed to result from Au precipitation which supports metallic gold surface bond formation.

Chapter 6: Suggestions for Future Work

This experimental investigation suggests Au doping via zinc cation substitution can be achieved. Being pivotal requirements for production of p-type ZnO films Au doped ZnO provides strong optimism for reliable bipolar doping. It is still unknown whether Au-doped ZnO films having multiphase and single phase structure exhibit n type or p type conduction. Structural results revealing high c –axis orientation is suggested to result from heteroepitaxial film growth. Although Au_{zn} lattice substitution has exceeded solubility for single phase film; Au impurity depth concentration must be understood to optimize growth conditions for allowable p-type behavior. Therefore, for future work it is imperative to perform electrical Hall measurements for carrier type and mobility, X-ray diffraction phi scan for epitaxial growth and SIMS depth profiling. Follow up analysis will assist in understanding whether Au-doped p-type ZnO has the potential to surmount the barrier, to full device implementation of ZnO.

Cited Literature

1. Y. Yan, M.Al-Jassim and Su-Huai Wei.Appl.Phys.Lett 89, 181912 (2006)
2. Kang,Ahn,Kim, Hee Kim,Lim, Chang and Lee. Appl Phys Lett 88, 202108 (2006)
3. Relva C. Buchanan. Ceramic Materials For Electronics 3rd edition, revised and expanded. Marcel Dekker Inc.(2004)
4. Ozgur,Alivov,Liu,Teke,Reschikov,Dogan,Avirutin,Cho and Morkoc. J. Appl. Phys. 98, 041301(2005)
5. W. Beyer. Thin Solid Films, 516 (2007) 147-154
6. Han, Theodore and Alford. J. Appl. Phys 103, 013708(2008)
7. Sivaramakhrishnan and Alford. Appl. Phys.Lett 94, 052104 (2009)
8. Singh,Mehra,Buthrath,Wakahara and Yoshida.J.Appl.Phys.90,5661(2001)
9. Yang, Beyermann,Katz, Ezekoye,Zuo, Pu,Shi, Pan and Liu. J. Appl.Phys. 105,053708 (2009)
10. Schwartz,Kittlstved and Gamelin.Appl.Phys.Lett 85, 1395 (2004)
11. Janotti and Van de Walle. Rep. Prog. Phys. 72 (2009) 126501
12. William Callister Jr and David G. Rethwisch, Fundamentals of Materials Science and Engineering, An integrated approach 3rd edition. Wiley and Sons (2007)
13. C.H. Park and D.J. Chadi. Phys.Rev.Lett.75,1134(1995)
14. D.C.Look and J.W.Hemsky.Phys. Rev.Lett 82,12(1999)
15. C.H.Park, S.B.Zhang and Su-Huai-Wei.Phys Rev. B 66,073202 (2002)
16. S.B. Zhang, S.H.Wei and Alex Zunger. Phys. Rev B 63,075205(2001)
17. Janotti and Van de Walle. Phys. Rev B 76, 165202(2007)
18. Fan, Sreekanth, Xie,Chang and Rao.Progress in Mat Sci 58(2013) 874-985
19. Hadis Morkoc and Umit Ozgur. Zinc Oxide(Fundamentals, Materials and Device Technology) Wiley-VCH (2009)
20. Raebiger,Lany and Zunger. Phys Rev B 76, 045209 (2007)
21. Tiwari, Snure,Kumar and Abiade. Appl.Phys.Lett 92, 062509 (2008)
22. Douglas B. Chrissey and Graham K. Hubler. Pulsed Laser Deposition of thin films. John C. Wiley and Sons (1994)
23. John C.Vickerman and Ian S. Gilmore. Surface Analysis:The Principle Technique. John wiley and sons (2009)
24. J.J Pireaux. Surface Science, 141 (1984) 221-232
25. Xiu, Yang, Mandalapu and L.Liu. Mater. Res.Soc.Symp.Proc.Vol.892 (2006)
26. Teke, Ozgur, Dogan, Gu and Morkoc. Phys Rev B, 70, 195207 (2004)